Available online at www.sciencedirect.com

ScienceDirect

Geochimica et Cosmochimica Acta 184 (2016) 257–271

Geochimica et Cosmochimica Acta

www.elsevier.com/locate/gca

# An experimental study on isotope fractionation in a mesoporous silica-water system with implications for vadose-zone hydrology

Ying Lin [a,b,*], Juske Horita [a,*]

[a] Department of Geosciences, Texas Tech University, Lubbock, TX 79409-1053, USA
[b] Institute of Deep-sea Science and Engineering, Chinese Academy of Sciences, Luhuitou Road No. 28, Sanya, Hainan 572000, China

Received 27 October 2015; accepted in revised form 18 April 2016; available online 27 April 2016

**Abstract**

Soil water dynamics within a thick vadose (unsaturated) zone is a key component in the hydrologic cycle in arid regions. In isotopic studies of soil water, the isotopic composition of adsorbed/pore-condensed water within soils has been assumed to be identical to that of bulk liquid water. To test this critical assumption, we have conducted laboratory experiments on equilibrium isotope fractionation between adsorbed/condensed water in mesoporous silica (average pore diameter 15 nm) and the vapor at relative pressures $p/p_o = 0.3$–$1.0$ along the adsorption–desorption isotherm at 30 °C. The isotope fractionation factors between condensed water in the silica pores and the vapor, $\alpha(^2H)$ and $\alpha(^{18}O)$, are smaller than those between liquid and vapor of bulk water (1.074 and 1.0088, respectively, at 30 °C). The $\alpha(^2H)$ and $\alpha(^{18}O)$ values progressively decrease from 1.064 and 1.0083 at $p/p_o = 1$ to 1.024 and 1.0044 at $p/p_o = 0.27$ for hydrogen and oxygen isotopes, respectively, establishing trends very similar to the isotherm curves. Empirical formulas relating $\alpha(^2H)$ and $\alpha(^{18}O)$ to the proportions of filled pores ($f$) are developed. Our experimental results challenge the long-held assumption that the equilibrium isotope fractionation factors for the soil water–vapor are identical to those of liquid water–vapor system with potential implications for arid-zone and global water cycles, including paleoclimate proxies in arid regions.


*Keywords:* Mesoporous silica; Adsorption-desorption isotherm; Equilibrium isotope fractionation factor; The Craig-Gordon evaporation model; Vadose-zone isotope hydrology

## 1. INTRODUCTION

Arid regions, generally classified based on mean annual precipitation (hyperarid, 0–50 mm; arid, 50–200 mm; and semiarid, 200–500 mm), constitute much of the Earth's land between latitudes 18° and 40° north and south of the equator, where the patterns of atmospheric circulation diverge or the lee sides of mountain chains create "rain shadows". These arid regions currently cover approximately 30% of the terrestrial land surface and account for a significant fraction of global net primary productivity (Grace et al., 2006). Under increasing human activities and the prospect of climate change, including reoccurring severe droughts in many parts of the globe, arid zones are ever expanding and becoming drier (e.g., Feng and Fu, 2013).

The land surface system in arid regions of terrestrial environments is located at a very critical interface within land–atmosphere–vegetation continuum of the energy-water

* Address: Department of Geosciences, Texas Tech University, Lubbock, TX 79409-1053, USA. Tel.: +1 (806)589 0922; fax: +1 (806)742 0100 (Y. Lin). Tel.: +1 (806)834 7027; fax: +1 (806)742 0100 (J. Horita).

*E-mail addresses:* ying.lin@ttu.edu (Y. Lin), Juske.horita@ttu.edu (J. Horita).

http://dx.doi.org/10.1016/j.gca.2016.04.029
0016-7037/

balance and ecological systems (Gat, 2010). The partitioning of precipitation and soil water into fluxes of percolation to the subsurface, surface runoff and evapotranspiration at the land–atmosphere–vegetation interface is accompanied by large changes in the stable isotopic ($\delta^2$H and $\delta^{18}$O) values, due to temporal and spatial variations in the isotopic compositions of precipitation events and the isotopic fractionation associated with the evaporation of water, both from open surface water and subsurface soil water (Gat, 2010). The two evaporation fluxes have distinct isotopic compositions and the latter becomes an increasingly dominant flux in arid regions (Good et al., 2015). On the other hand, the isotopic composition of the transpiration flux is very similar to that of soil water since the uptake by plant roots is usually not associated with isotope fractionation (Flanagan and Ehleringer, 1991). Thus, the isotopic compositions of soil water and evaporation flux are the key parameters for our understanding of the land–atmosphere–vegetation interface in arid regions.

Soil pore space, which is the void within and between soil particles, is a continuum of pores whose sizes and shapes vary extremely. Recent studies revealed (Hajnos et al., 2006; Ferreiro et al., 2010; Lu et al., 2014) that soil pore sizes range from smaller than nanometers within soil particles to the order of centimeters in shrinkage cracks. Clay minerals also constitute a large fraction of matured soils with interlayers in the range of 1–2 nm. In arid regions strong evaporation from the surface dramatically decreases the water content of soil much below the saturation value. Many observations in desert vadose zones in the U.S. Southwest and elsewhere (Scanlon et al., 1997; Scanlon, 2000; Flint et al., 2002; Duniway et al., 2007) show extremely negative matric potentials of water (−10 to −100 MPa) near the surface due to strong evaporation from the soil surface. Under such dry conditions, large interparticle pores are quickly drained and other mechanisms of water adsorption in soils become dominant, including mono-/multi-layer films on grain surfaces, narrow pore throats, intraparticle pores, and clay interlayer pores. The total reservoir capacity of the "tight" water is probably limited, but large and varying fluxes of water vapor within thick vadose zones make "tight" water an active and crucial component of the water cycle in arid regions.

The structural layers of clay minerals have permanent negative charges, counter-charged by exchangeable cations. These cations adsorbed to clay particles interact with surrounding water and change their properties, including isotope ratios. Stewart (1972) performed experiments on $^2$H/$^1$H isotopic fractionation between adsorbed water in clays and water vapor. He determined the equilibrium fractionation factors $\alpha = (^2\mathrm{H}/^1\mathrm{H})_{\mathrm{adsorbed\ water}}/(^2\mathrm{H}/^1\mathrm{H})_{\mathrm{vapor}}$ to be 0.93–1.06 with a median of 1.04, which are significantly lower than that for bulk liquid water–vapor system with $\alpha_{L-V} = 1.079$ at 25 °C (Horita and Wesolowski, 1994). Oxygen isotope fractionation effects in the homoionic smectite-water mixture were found to be positive for $Mg^{2+}$ and $Ca^{2+}$ exchanged smectites and negative for $K^+$ exchanged smectite relative to the added water and these isotope effects increase with decreasing water contents (Oerter et al., 2014). Coplen and Hanshaw (1973) found that hydrogen and oxygen isotopes fractionated in the ultrafiltration experiments through a compacted clay membrane.

Oxides such as silica and alumina are major chemical components of soil minerals. Richard et al. (2007) carried out an experimental study on adsorbed water inside porous silica tubes (10–16 nm pore diameter) at 20 °C and found significantly lower $^2$H/$^1$H fractionation factors between adsorbed water and water vapor ($\alpha = 1.03$ and 1.065 at 10 and 85% relative humidity, respectively) relative to the bulk water ($\alpha_{L-V} = 1.084$ at 20 °C, Horita and Wesolowski, 1994). Channel water in various micropore (<2 nm) zeolite minerals (analcime, wairakite, chabazite, laumonite, and modernite) may serve as an analog to capillary condensed water in soil minerals. Limited and inconclusive experimental studies (Karlsson and Clayton, 1990; Feng and Savin, 1993; Noto and Kusakabe, 1997; Karlsson, 2001) suggest that channel water is depleted in both $^{18}$O and $^2$H relative to bulk water at near ambient temperature, except for modernite.

The objective of this study is to test the hypothesis that equilibrium isotope fractionation between adsorbed/pore-condensed water within soils and water vapor differs significantly from that of the bulk liquid water–water vapor system ($\alpha_{L-V}$) at the same temperature, due to complex hydrophilic interactions between the soil surface and water molecules. We conducted a series of laboratory experiments to systematically and accurately determine the associated $^2$H/$^1$H and $^{18}$O/$^{16}$O isotope fractionation factors between adsorbed/condensed water in a mesoporous silica sample and water vapor from very low vapor pressure to near the saturation pressure.

## 2. MATERIAL AND EXPERIMENTAL SETUP

### 2.1. Material

Soils are mixtures of various minerals of different compositions, sizes, and textures, including organic matter and bacteria. These natural soils are too complex to use in this experimental study. Quartz grains are often used in soil physics studies (e.g., Ottawa sand and Accusand), but they have low surface areas with very limited internal pores (<0.1 m$^2$/g). Mesopores (2–50 nm, as defined by the International Union of Pure and Applied Chemistry, IUPAC) are our main interest as soil analog materials because of: (a) an increasing recognition of their occurrence in soils and various rock types (Gruszkiewicz et al., 2001; Hajnos et al., 2006; Chen et al., 2007; Nielsen and Fisk, 2010) and (b) their strong hysteresis in adsorption–desorption isotherm of water over a wide range of the water activity ($p/p_o$ where $p_o$ is the saturation pressure). Macropores (>50 nm) fill up only at near saturation and micropores (<2 nm) are not of relevance except at extremely dry conditions ($p/p_o < 0.2$).

We used a high-purity grade amorphous silica sample with an average pore diameter of 15 nm from Sigma–Aldrich (CAS No. 112926-00-8, Product No. 243981, Davisil Grade 62, 15 nm pore diameter, 75–250 μm particle size, pore volume 1.15 cm$^3$/g, surface area 300 m$^2$/g). The characteristics of simple chemical composition and variable,

yet controlled pore size distributions make mesoporous silica materials excellent analog materials for natural soils. When fully hydroxylated, the surface of amorphous silica is covered with several types of silanol groups (≡Si—OH).

### 2.2. Experimental setup

An experimental system for water adsorption–desorption was built mainly of Pyrex glass and is evacuated with mechanical and diffusion pumps down to $<10^{-3}$ Torr (Fig. 1). The equilibration unit consists of a lower flask for adsorbent solids and an upper glass bulb (5 L) for adsorptive water vapor, which are separated by a large-bore Teflon stopcock. The lower flask is specially designed to have a small petri dish in the center to hold the porous material and leave enough space at the bottom for a magnetic stir bar to mix the water vapor between the upper and lower chambers. The lower part of the equilibration unit was controlled at 30 ± 0.1 °C by a water bath. We have chosen the experimental temperature of 30 °C since it is close to soil temperature in arid regions and can be readily controlled in laboratory. The glass bulb and the glass vacuum line were wrapped by heating elements to a slightly higher temperature (30–35 °C) to avoid condensation. The vapor pressure inside the equilibration unit can be determined to a precision of 0.01 Torr with a MKS Baratron capacitance manometer. To the right side of the equilibration unit, water of a known amount was injected by a syringe through the septum port, then the air introduced was evacuated after freezing the water with liquid nitrogen ($LN_2$), finally the water was transferred into the equilibration unit. To the left side of the equilibration unit, water vapor in the upper glass bulb and adsorbed water in the lower flask of the equilibration unit can be separated by closing the large stopcock, frozen into a U-trap and transferred to Pyrex sample tubes separately. The equilibration unit was tested by liquid–vapor equilibration of bulk water. At 30.0 ± 0.1 °C, saturation vapor pressure of 31.85 Torr was observed, which agrees well with the literature value of 31.88 ± 0.2 Torr (Harvey, 1998).

## 3. CHARACTERIZATION OF MESOPOROUS SILICA

### 3.1. Scanning electron microscopy

An electron micrograph of the mesoporous silica gel was obtained by Hitachi SEM S-5000 scanning electron microscopy at 3 kV in scanning mode (Fig. 2). Before the imaging, the silica sample powders were fixed onto a piece of carbon tape and coated with iridium to minimize charging. From Fig. 2, the silica particles are typically spherical and relatively evenly sized. Pores with diameters of ~10–20 nm occupy space between the silica particles.

### 3.2. Adsorption–desorption isotherm

To remove any adsorbed salts on the silica gel and fully hydroxylate its surface, about 10 g of the silica sample was

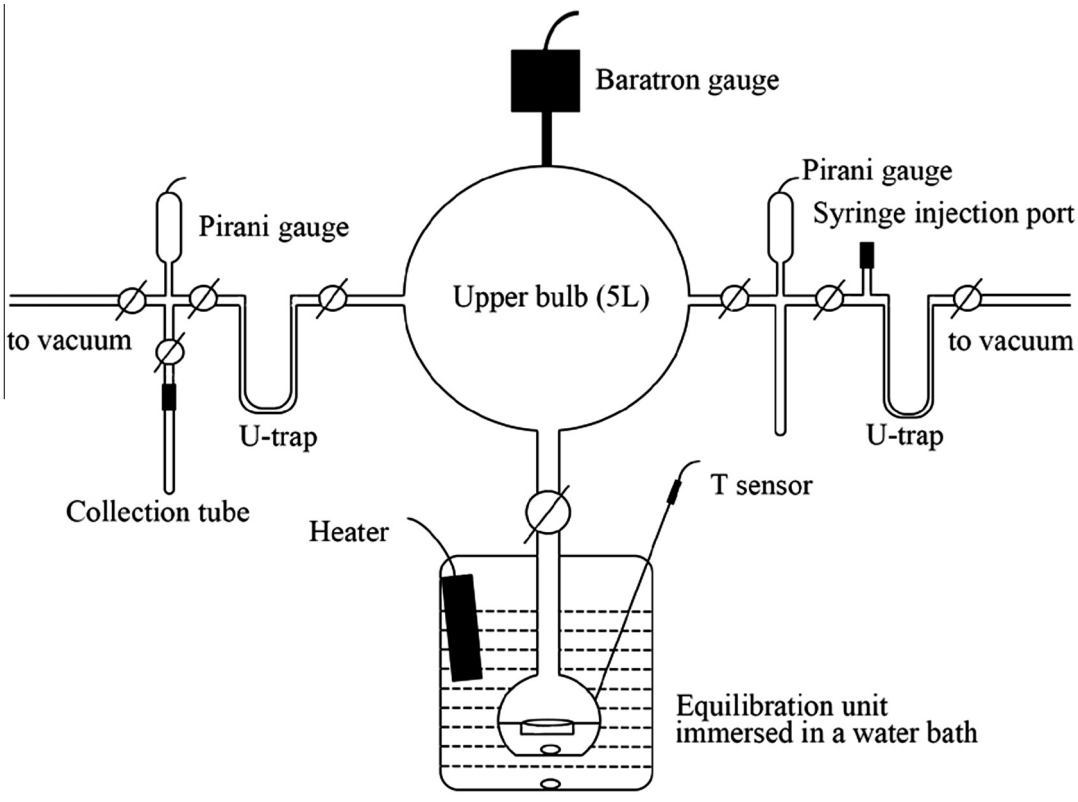


Fig. 1. The experimental setup for determining the adsorption–desorption isotherm of water and the isotope fractionation factors between water vapor and adsorbed water on silica.

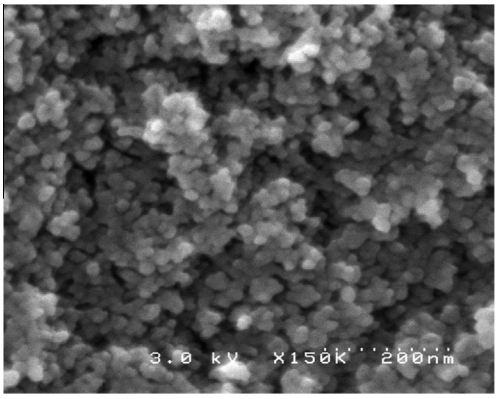


Fig. 2. An SEM image of mesoporous silica (15 nm) sample (Davisil Grade 62).

fully soaked in W-1 water (nanopure water from Oak Ridge National Laboratory) with an isotopic composition of −42.0‰ ($\delta^2$H) and −6.8‰ ($\delta^{18}$O). After several days, the water was decanted and the porous silica gel was dried in a desiccator at room temperature with phosphorous oxide ($P_2O_5$) as a desiccant to avoid dehydroxilation of the silica surface.

*3.2.1. Nitrogen isotherm*

An $N_2$ adsorption–desorption isotherm at $LN_2$ temperature (−196 °C) was determined for the silica sample using a Quantachrome NOVA 2200*e* analyzer. Specific surface areas were determined by the multipoint Brunauer, Emmett and Teller (BET) method using NOVA Win2 software. Total pore volume and average pore size can be calculated by different methods within NOVA (Table 1).

*3.2.2. Water isotherm*

Once the surface of the porous silica gel is fully hydroxylated as described above, physisorption (reversible adsorption, in which the forces involved are intermolecular van der Waals forces rather than valence forces) is the main mechanism of water adsorption. It has been reported that this physisorption of water is totally reversible, and the hystereses of water adsorption–desorption on the mesoporous materials close (Gregg and Sing, 1982; Naono and Hakuman, 1991, 1993; Naono et al., 2000; Likos and Lu, 2006; Likos et al., 2011). The closure of hysteresis is of critical importance in conducting experiments for accurately determining isotope effects in the adsorption–desorption and capillary condensation of water molecules in soil and other geologic materials.

The adsorption–desorption isotherm of water on the silica (15 nm pore diameter) was determined in the entire range of $p/p_o = 0$–1. The purpose is to determine the amounts of water adsorbed on the samples and the extent of adsorption–desorption hysteresis as a function of $p/p_o$. Only about one monolayer of water is adsorbed on the surface of new Pyrex glass when vapor pressure is 50% of saturated value (Burnett et al., 1996). This amount of water adsorption on the inner wall of the equilibration unit ($\sim 5 \times 10^{-2}$ mg in a 5 L bulb) is negligible. After loading a pretreated sample (hydroxylated by W-1 water and desiccated by $P_2O_5$) into the petri dish of the lower flask, the entire system was evacuated to $<10^{-3}$ Torr to remove all physisorbed water. A $LN_2$ dewer was loaded under the U-trap to facilitate this process. Then, a given amount (10–100's of mg) of the W-1 water was introduced over 20 steps to the equilibration unit until $p/p_o = 1$. At each step, the pressure within the equilibration unit was monitored until the pressure became stable (about 2–4 h). The amount of water adsorbed on the silica gel at each step was calculated by subtracting the amount of water vapor determined by the ideal-gas law from the total amount of water injected. An entire adsorption isotherm was thus constructed incrementally from $p/p_o = 0$ upwards. After reaching $p/p_o = 1$, the desorption curve was also determined by withdrawing a small amount of water vapor out of the equilibration unit to a Pyrex finger tube for weighing and by recording the stabilized pressure in the unit until $p/p_o = 0$.

## 4. EXPERIMENTS FOR ISOTOPE EFFECTS ASSOCIATED WITH WATER ADSORPTION

After determining the adsorption–desorption isotherm of water on the silica sample, a series of separate experiments was carried out with the purpose of determining isotope effects associated with the condensation of water in pores of the mesoporous silica sample at 30 °C. After equilibration, samples of water vapor and adsorbed water on the mesoporous silica were collected in Pyrex finger tubes. Then the water samples were immediately transferred into 2 ml autosampler vials for isotope analyses. If the analyses were not done the same day, the water samples were flame-sealed inside the finger tubes. Each water sample was injected by a PAL autosampler into a Finnigan™ TC/EA high-temperature reactor to convert water to carbon monoxide (CO) and hydrogen gas ($H_2$) at 1390 °C, which were further analyzed by a Finnigan™ Delta V Plus Isotope Ratio Mass Spectrometer (IRMS). We set up the autosampler to rinse the syringe with a water sample several times

Table 1
The properties of the mesoporous silica (average pore diameter of 15 nm) determined from $N_2$ and water adsorption–desorption isotherms.

| Adsorptive | Total pore volume (cc/g) | Average pore diameter (nm) | Specific surface area ($m^2$/g) | Method used |
|---|---|---|---|---|
| $N_2$ | | | 302.94 | Multipoint BET |
| | 1.11 | | | |
| | | 14.70 | | |
| | 1.09 | 15.18 | 276.8 | BJH (adsorption branch) |
| Water | 1.13 | 14.0 | 293.8 | Kelvin Equation (desorption branch) |

and to carry out several flush injections to get rid of memory effects within the TC/EA reactor. A set of SMOW (Standard Mean Ocean Water) and SLAP (Standard Light Antarctic Precipitation) standards was run daily in order to normalize the data to the SMOW–SLAP scale. The internal precisions (standard deviation of 5–6 analytical runs of the same sample) of $\delta^2$H and $\delta^{18}$O values are generally $<\pm1‰$ and $<\pm0.1‰$ ($1\sigma$), respectively. The precisions of isotopic fractionation factors, $\alpha(^2\text{H})$ and $\alpha(^{18}\text{O})$, are $\pm0.001$ and $\pm0.0001$ ($1\sigma$), respectively, where:

$$\alpha = \frac{1+\delta_{\text{Adsorbed water}}}{1+\delta_{\text{Vapor}}} \quad (1)$$

### 4.1. Isotopic integrity

In addition to the quantitative recovery of water, possible isotope exchange between adsorbed water and the surface ─OH group of the mesoporous silica is a major concern. Thus, the isotopic integrity of the adsorbed water is also a prerequisite to the accurate measurements of isotope effects in adsorption–desorption in mesoporous materials. We investigated the isotopic integrity of water in adsorption and desorption processes by first introducing a given amount of water with a known isotopic composition (W-1 water in this study) to reach a given $p/p_o$ value along the adsorption curve and then recovering water vapor and the adsorbed water together. We carried out an experiment at a relative pressure of $p/p_o = 0.8$, and found the recovered water to have $\delta^2$H and $\delta^{18}$O values of $-41.49‰$ and $-6.69‰$, respectively, identical to the W-1 isotopic composition of $-41.97‰$ and $-6.82‰$ within experimental uncertainties. This criterion of isotopic integrity was applied to all experimental data reported in this study.

### 4.2. Isotope equilibration

The attainment of equilibrium of physical adsorption–desorption of water, which can be readily monitored by the changes in vapor pressure, took from 2 to 4 h, but isotope equilibrium between water vapor and adsorbed water is expected to take longer to reach. Richard et al. (2007) showed that hydrogen isotope equilibrium was reached between about 4 and 17 h depending on the vapor pressure. In this study, we carried out isotope equilibrium experiments first to determine the duration of time that it takes to reach steady values of both oxygen and hydrogen isotopic fractionation factors between water vapor and adsorbed water in the mesoporous silica (15 nm), then to verify the attainment of isotopic equilibrium by an isotopic reversal experiment using waters of different isotopic compositions (O'Neil, 1986).

In the first set of experiments, a given amount of W-1 water was introduced into the equilibration unit containing the silica sample to reach $p/p_o = 0.9$. After selected time durations, the upper bulb and the lower flask were isolated, and then water vapor and the adsorbed water were extracted separately. We varied the equilibration time at 19 h, 41 h, and 89 h, and found the values of $\alpha(^2\text{H})$ and $\alpha(^{18}\text{O})$ were constant within uncertainties: 1.058, 1.057, 1.061 and 1.0080, 1.0078, 1.0081, respectively.

In the isotope reversal experiment, in which waters of different isotopic compositions are used to approach an equilibrium isotope fractionation from opposite directions (O'Neil, 1986), W-1 water was first introduced into the equilibration unit containing the silica sample to reach $p/p_o = 0.78$. After ~48 h of equilibration, the upper bulb and the lower flask were isolated and the vapor in the upper bulb was extracted, leaving the adsorbed water on the silica gel intact. Then, Edmonton, Alberta tap water ($\delta^2\text{H} = -154.94‰$, $\delta^{18}\text{O} = -19.66‰$) was injected into the equilibration unit to reach the same vapor pressure with an initial isotope fractionation factor between the adsorbed W-1 water and Edmonton water vapor much larger than the expected equilibrium value. After ~48 h of equilibration, the vapor and the adsorbed water were extracted separately and were analyzed for both oxygen and hydrogen isotopic compositions. A second part of the isotope reversal experiment was similar to the first one, also at a vapor pressure $p/p_o = 0.78$ but injecting W7 water ($\delta^2\text{H} = 24.36‰$, $\delta^{18}\text{O} = 2.07‰$) instead of Edmonton water. This gave a much smaller initial isotope fractionation factor between the adsorbed W-1 water and W7 water vapor, relative to an equilibrium value. After equilibration, the oxygen and hydrogen isotopic fractionation factors measured for the subsets of isotope reversal experiment were very close: $\alpha(^2\text{H}) = 1.060$ and $1.059$, $\alpha(^{18}\text{O}) = 1.0084$ and $1.0081$ for Edmonton and W7 injections, respectively, verifying that isotope equilibrium was attained after a duration of ~48 h, or approximately two days (Fig. 3).

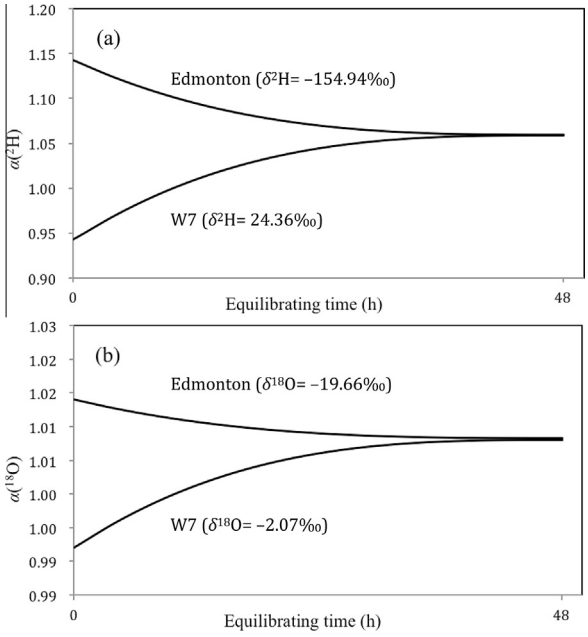


Fig. 3. The isotope reversal experiment: converging of isotopic fractionation factors over ~48 h from the introduction of a heavy (W7) and a light (Edmonton) water into the equilibration unit that contained W-1 adsorbed in silica sample. (a) $\alpha(^2\text{H})$; (b) $\alpha(^{18}\text{O})$. The curves show general trends only.

Table 2
The experimental results at 30 °C to determine the isotope fractionation factors (α) between adsorbed water in silica (15 nm) and water vapor. Fractionation factors of liquid–vapor equilibrium of bulk water are also listed for comparison.

| | | $\delta^2$H (‰) | $\delta^{18}$O (‰) | Amount of adsorbed water[†] (g/g-silica) | Corrected $\delta^2$H[‡] (‰) | Corrected $\delta^{18}$O[‡] (‰) | $\alpha(^2H)$ | $\alpha(^{18}O)$ | Pressure (Torr) | Relative pressure ($p/p_o$) | $\ln[\alpha(^2H)]/\ln[\alpha(^{18}O)]$ | Pore filled ($f$) |
|---|---|---|---|---|---|---|---|---|---|---|---|---|
| L–V eq. #1 | Liq | −40.06 | −6.81 | – | – | – | 1.0740 | 1.0088 | 31.85 | 1 | 8.15 | – |
| | Vap | −106.2 | −15.47 | – | – | – | | | | | | |
| L–V eq. #2 | Liq | −39.67 | −6.65 | – | – | – | 1.0756 | 1.0090 | 31.85 | 1 | 8.13 | – |
| | Vap | −107.18 | −15.47 | – | – | – | | | | | | |
| Exp#1 | Ads[§] | −27.59 | −4.81 | 1.07 | −25.90 | −4.57 | 1.06381 | 1.00831 | 31.88 | 1.00 | 7.48 | 0.96 |
| | Vap[**] | −84.33 | −12.78 | 0.35 | −84.33 | −12.78 | | | | | | |
| Exp#2 | Ads | −28.44 | −4.91 | 1.02 | −26.71 | −4.67 | 1.06366 | 1.00815 | 31.15 | 0.97 | 7.61 | 0.92 |
| | Vap | −84.96 | −12.71 | 0.34 | −84.96 | −12.71 | | | | | | |
| Exp#3 | Ads | −26.85 | −4.66 | 1.00 | −25.09 | −4.41 | 1.06494 | 1.00831 | 30.4 | 0.95 | 7.60 | 0.9 |
| | Vap | −84.53 | −12.62 | 1.07 | −84.53 | −12.62 | | | | | | |
| Exp#4 | Ads | −34.14 | −5.64 | 0.98 | −33.01 | −5.48 | 1.06412 | 1.00827 | 29.14 | 0.91 | 7.55 | 0.88 |
| | Vap | −91.28 | −13.64 | 0.17 | −91.28 | −13.64 | | | | | | |
| Exp#5 | Ads | −30.70 | −5.53 | 0.67 | −29.12 | −5.31 | 1.06313 | 1.00817 | 27.98 | 0.87 | 7.52 | 0.60 |
| | Vap | −86.77 | −13.37 | 0.17 | −86.77 | −13.37 | | | | | | |
| Exp#6 | Ads | −30.25 | −5.13 | 0.59 | −28.46 | −4.88 | 1.06006 | 1.00780 | 27.6 | 0.86 | 7.51 | 0.53 |
| | Vap | −83.50 | −12.59 | 0.18 | −83.50 | −12.59 | | | | | | |
| Exp#7 | Ads | −27.13 | −5.15 | 0.53 | −25.22 | −4.89 | 1.06231 | 1.00799 | 27.6 | 0.86 | 7.60 | 0.47 |
| | Vap | −82.40 | −12.78 | 0.17 | −82.40 | −12.78 | | | | | | |
| Exp#8 | Ads | −25.82 | −4.55 | 0.38 | −23.33 | −4.21 | 1.05769 | 1.00732 | 27.48 | 0.86 | 7.69 | 0.34 |
| | Vap | −76.60 | −11.45 | 0.17 | −76.60 | −11.45 | | | | | | |
| Exp#9 | Ads | −24.09 | −4.17 | 0.27 | −20.94 | −3.71 | 1.05460 | 1.00751 | 26.9 | 0.84 | 7.11 | 0.24 |
| | Vap | −71.63 | −11.14 | 0.16 | −71.63 | −11.14 | | | | | | |
| Exp#10 | Ads | −33.63 | −4.74 | 0.33 | −31.92 | −4.47 | 1.04485 | 1.00645 | 26.12 | 0.82 | 6.82 | 0.30 |
| | Vap | −73.48 | −10.85 | 0.15 | −73.48 | −10.85 | | | | | | |
| Exp#11 | Ads | −28.24 | −4.74 | 0.26 | −26.30 | −4.43 | 1.04068 | 1.00610 | 25.16 | 0.79 | 6.56 | 0.23 |
| | Vap | −64.36 | −10.46 | 0.15 | −64.36 | −10.46 | | | | | | |
| Exp#12 | Ads | −32.32 | −4.67 | 0.19 | −30.35 | −4.34 | 1.03776 | 1.00600 | 23.33 | 0.73 | 6.20 | 0.17 |
| | Vap | −65.63 | −10.28 | 0.13 | −65.63 | −10.28 | | | | | | |
| Exp#13 | Ads | −26.76 | −4.44 | 0.08 | −24.56 | −4.06 | 1.03451 | 1.00555 | 21.2 | 0.66 | 6.13 | 0.07 |
| | Vap | −57.10 | −9.56 | 0.06 | −57.10 | −9.56 | | | | | | |
| Exp#14 | Ads | −32.44 | −4.68 | 0.07 | −30.42 | −4.29 | 1.02960 | 1.00542 | 19.95 | 0.62 | 5.40 | 0.06 |
| | Vap | −58.30 | −9.66 | 0.06 | −58.30 | −9.66 | | | | | | |
| Exp#15 | Ads | −33.49 | −4.59 | 0.06 | −31.53 | −4.20 | 1.02774 | 1.00527 | 17.13 | 0.54 | 5.21 | 0.05 |
| | Vap | −57.67 | −9.42 | 0.05 | −57.67 | −9.42 | | | | | | |

| | | | | | | | | | | | | |
|---|---|---|---|---|---|---|---|---|---|---|---|---|
| Exp#16 | Ads | −33.23 | −4.93 | 0.05 | | −31.25 | −4.55 | 1.02759 | 1.00501 | 15.32 | 0.48 | 5.45 | 0.04 |
| | Vap | −57.26 | −9.52 | 0.05 | | −57.26 | −9.52 | | | | | | |
| Exp#17 | Ads | −30.49 | −4.79 | 0.05 | | −28.74 | −4.47 | 1.02608 | 1.00453 | 13 | 0.41 | 5.70 | 0.04 |
| | Vap | −53.42 | −8.96 | 0.04 | | −53.42 | −8.96 | | | | | | |
| Exp#18 | Ads | −29.75 | −4.88 | 0.04 | | −28.19 | −4.59 | 1.02460 | 1.00449 | 10.7 | 0.33 | 5.42 | 0.04 |
| | Vap | −51.52 | −9.04 | 0.03 | | −51.52 | −9.04 | | | | | | |
| Exp#19 | Ads | −31.74 | −4.86 | 0.04 | | −30.42 | −4.60 | 1.02353 | 1.00444 | 8.48 | 0.27 | 5.25 | 0.03 |
| | Vap | −52.71 | −9.00 | 0.03 | | −52.71 | −9.00 | | | | | | |

† After equilibration, the upper bulb and the lower flask were isolated and water vapor and adsorbed water were extracted separately. However, since the lower flask contained a small amount of water vapor, a volume correction is applied to the amounts of adsorbed water collected.
‡ After correction for water vapor in the lower flask.
§ Represents adsorbed water in silica.
** Represents water vapor.

### 4.3. Determination of equilibrium fractionation factors

After verifying the isotopic integrity and the attainment of isotopic equilibrium in the adsorption–desorption process, we determined equilibrium $^{2}H/^{1}H$ and $^{18}O/^{16}O$ isotope fractionation factors between water vapor and the adsorbed water as a function of $p/p_o$ ($p/p_o = 0.3$–$1.0$) along the adsorption isotherm. These values should cover conditions for soils in semiarid to arid regions. For each experiment, a specific amount of W-1 water was injected and transferred into the equilibration unit containing a specific amount of the silica. After two days of equilibration, water vapor and adsorbed water were recovered for isotopic analysis. Since the isolation of the upper bulb and the lower flask before the collection leaves some vapor in the lower flask, we applied small corrections to the amounts of water vapor and adsorbed water collected and to the isotopic composition of the adsorbed water (Table 2).

## 5. RESULTS

### 5.1. Adsorption–desorption isotherms

Both $N_2$ and water isotherms of the silica sample (15 nm) (Figs. 4 and 5) show type IV isotherm and Type H1 hysteresis based on the IUPAC classification (Sing et al., 1985). Type IV isotherm is typically found for mesoporous adsorbents. The initial part is attributed to monolayer–multilayer adsorption, the hysteresis loop is associated with capillary condensation, and the plateau part indicates limiting uptake at high $p/p_o$. In type H1 hysteresis, the two branches are almost vertical and nearly parallel over a wide range of $p/p_o$. A feature common to many hysteresis loops is that the steep region of the desorption branch leading to the lower closure point occurs at a relative pressure which depends mainly on the nature of the adsorptive gas (Sing et al., 1985).

At low pressures ($p/p_o = 0$–$0.4$), an adsorbate monolayer of $N_2$ or water is first formed on the pore surface of the silica gel, followed by the multilayer formation. The number of molecules adsorbed on the external sample surface is negligible in comparison to the pore walls, due to the very large internal surface of the mesoporous silica gel (Gregg and Sing, 1982). The onset of the hysteresis loop at $p/p_o = 0.4$ (water) or 0.6 ($N_2$) marks the beginning of the capillary condensation in the pores (15 nm diameter). The closure of hysteresis in the water adsorption–desorption isotherm at $p/p_o = 0.4$ is an indication of quantitative recovery of the adsorbed water. The lower closure point of hysteresis for water relative to that for $N_2$ is probably due to the difference in their molecular sizes (water: ~2.75 Å and $N_2$: ~3.00 Å). At the external vapor pressure corresponding to the upper closure point of the hysteresis loop ($p/p_o = 0.95$), the pores are completely filled with liquid. Diffusion processes also vary along the isotherm (Naumov, 2009).

The properties of the silica sample calculated from the desorption branch of the water isotherm using a method based on the Kelvin equation (Lowell et al., 2010), together with the material properties calculated from the $N_2$-silica

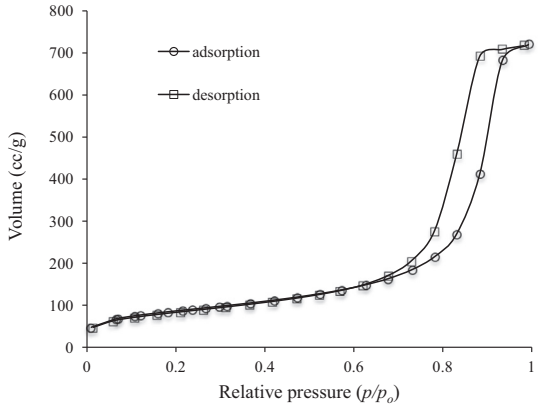


Fig. 4. The adsorption–desorption isotherm of $N_2$ on mesoporous silica (15 nm).

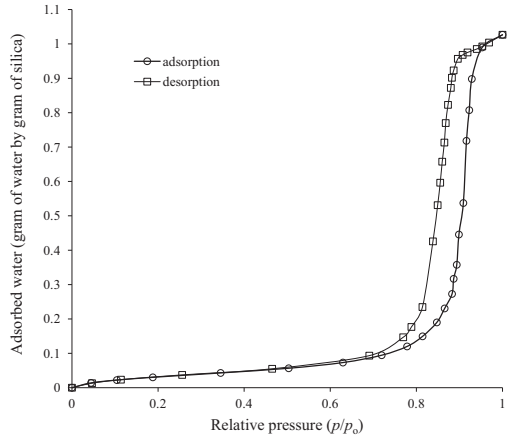


Fig. 5. The adsorption–desorption isotherm of water on mesoporous silica (15 nm).

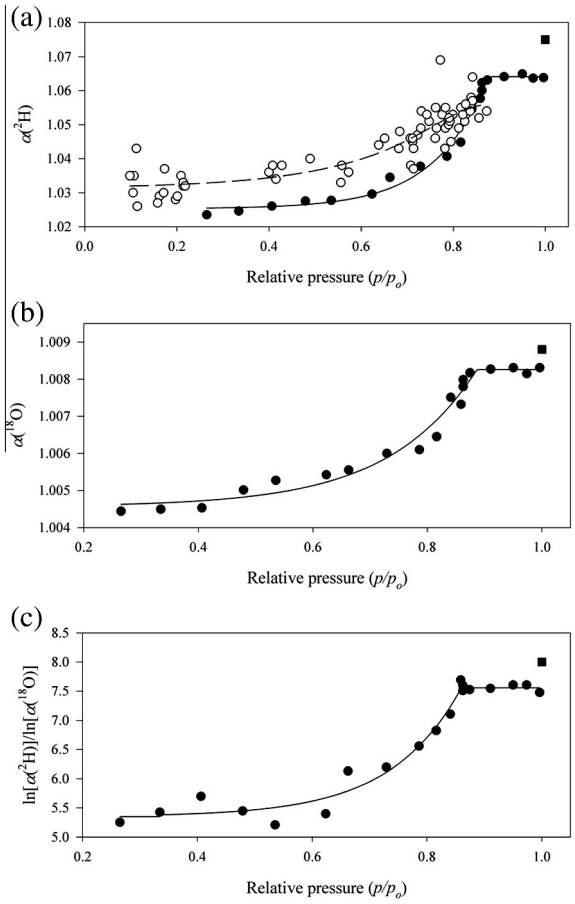


Fig. 6. Isotope fractionation factors (α) between water vapor and adsorbed water in silica (15 nm) at 30 °C with varying relative pressures ($p/p_o$): (a) $\alpha(^2H)$. Data from Richard et al. (2007) are shown in the open circles; (b) $\alpha(^{18}O)$; (c) $\ln[\alpha(^2H)]/\ln[\alpha(^{18}O)]$. The solid squares represent data for bulk water liquid–vapor fractionation. The solid and dashed lines are for guidance only.

isotherm, are summarized in Table 1. Different methods give consistent results with average pore diameters of 14–15.2 nm and specific surface areas of 277–303 $m^2/g$. Based on the $N_2$-silica isotherm, pore radii are found to spread the range of 3–160 Å with a sharp peak at 75 Å, or 7.5 nm.

### 5.2. Equilibrium isotope fractionation

We first carried out experiments to determine equilibrium isotope fractionation factors for bulk water. The results from two liquid–vapor (L–V) equilibration experiments of bulk water show that average values of $\alpha_{L-V}(^2H)$ and $\alpha_{L-V}(^{18}O)$ at 30 °C are 1.075 and 1.0089, respectively (Table 2). These values are identical within experimental uncertainties to those of Horita and Wesolowski (1994) (1.074 and 1.0089, respectively).

We present the results only from the experiments that had quantitative recovery of water (within a mass fraction of 0.3%) and attained the isotope integrity of both oxygen and hydrogen (mostly within ±2 and ±0.2‰ for $\delta^2H$ and $\delta^{18}O$, respectively) (Table 2 and Fig. 6). The equilibrium isotope fractionation factors, $\alpha(^2H)$ and $\alpha(^{18}O)$, between adsorbed water and water vapor increase from 1.024 to 1.063 and from 1.0044 to 1.0082, respectively, with $p/p_o$ rising from 0.27 to 0.87. Afterward, the fractionation factors do not vary much. At $p/p_o$ very close to 1, $\alpha(^2H)$ and $\alpha(^{18}O)$ are 1.064 and 1.0083, respectively. These values are lower than those of liquid–vapor (L–V) equilibration of pure water (Fig. 6). The changes in the fractionation factors with varying $p/p_o$ are quite similar to the adsorption isotherm, with an exponential rise at the region of hysteresis and a plateau approaching saturation.

The only relevant literature study is Richard et al. (2007), in which equilibrium $^2H/^1H$ fractionation factors between water vapor and adsorbed water on porous silica tubes at room temperature were determined. The average pore diameter of the silica tubes (12–16 nm) is similar to the silica used in this study. The experimental precision for $\delta^2H$ is ±2‰, and oxygen isotopic compositions were not determined due to the low amount of the extracted water. The variation of $\alpha(^2H)$ with $p/p_o$ exhibited a trend similar to ours (from 1.025 at $p/p_o = 0.1$ to 1.065 at

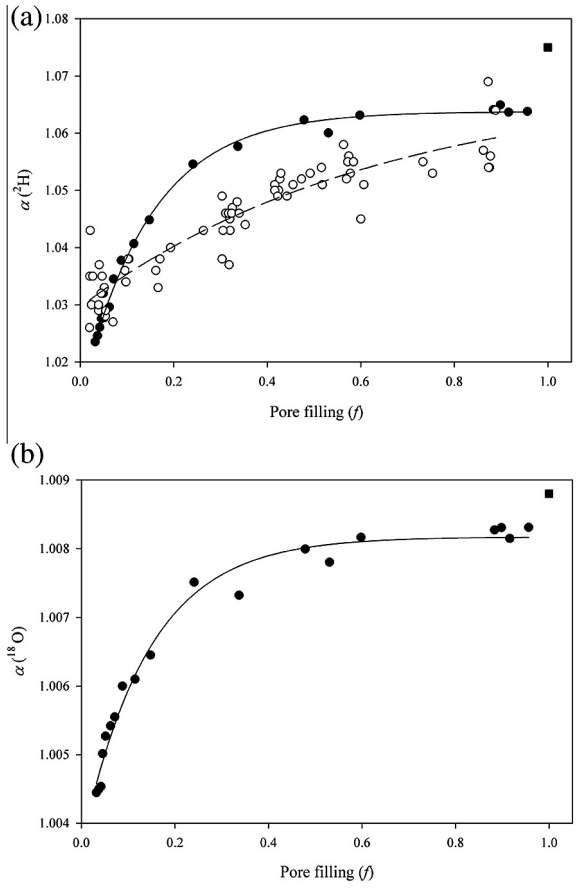


Fig. 7. The exponential increase of α values with increasing proportions of the pores filled ($f$) at 30 °C: (a) $\alpha(^2H)$. Data from Richard et al. (2007) are shown in the open circles and are fitted with a dashed curve; (b) $\alpha(^{18}O)$. The solid squares represent data for bulk water liquid–vapor fractionation taking $f = 1$. See Eqs. (2) and (3) for the fitted solid curves.

$p/p_o = 0.85$), showing a steep slope at the region of hysteresis (Fig. 6a). However, due to the relatively low precision and the range of $p/p_o$ explored by Richard et al. (2007), the trend was not smooth and the plateau approaching the saturation vapor pressure was not observed. The variation of $\alpha(^2H)$ with water quantity also exhibited a similar trend to ours, but again, much more scattered (Fig. 7a).

The change of $\ln[\alpha(^2H)]/\ln[\alpha(^{18}O)]$ values with $p/p_o$ exhibits a similar trend, with an exponential rise at the region of hysteresis and a plateau approaching saturation (Fig. 6c). The values of $\ln[\alpha(^2H)]/\ln[\alpha(^{18}O)]$ increase from 5.25 at $p/p_o = 0.27$ to ~7.60 at $p/p_o \geqslant 0.85$, and then remain nearly constant. These values are lower than the average $\ln[\alpha(^2H)]/\ln[\alpha(^{18}O)]$ value of bulk water of 8.14.

Fig. 7 shows that $\alpha(^2H)$ and $\alpha(^{18}O)$ values increase rapidly with increasing proportions of pore filled ($f$, volume fraction of water-filled pores over total pores). With increasing $f$ from 0.03 to 0.96, $\alpha(^2H)$ and $\alpha(^{18}O)$ values increase asymptotically from 1.024 to 1.064 and from 1.0044 to about 1.0083, respectively (Table 2):

$$\alpha(^2H) = 1.0140 + 0.0498 \cdot (1 - e^{-6.7392 \cdot f}) \quad (2)$$

$$\alpha(^{18}O) = 1.0037 + 0.0045 \cdot (1 - e^{-6.9975 \cdot f}) \quad (3)$$

All of the above results strongly suggest that the equilibrium fractionation factors between adsorbed water in pores of the mesoporous silica (15 nm) and water vapor are lower than those of bulk water at 30 °C, and decrease with decreasing relative pressures ($p/p_o$) or water contents in the pores.

## 6. DISCUSSION

### 6.1. Structure and dynamics of interfacial/confined water

The intermolecular hydrogen bond of bulk liquid water is established between two oxygen atoms through a proton and the electronic distribution called a "lone pair", which is due to the hybridation of the electronic orbitals (Bellissent-Funel, 2008). A high directionality of H-bond gives rise to a locally tetrahedral coordination of water molecules (Walrafen, 1981). The microscopic structure of "confined water" or "interfacial water" in porous geologic (soil, rock, clay minerals), engineered (zeolite and other mesoporous catalysts), and biological materials (living cells and membranes) is modified by the distortion of hydrogen bonds among the water molecules and more extensive hydrogen bonding with the pore surfaces. In the case of porous silica, hydrophilic silanol groups (≡Si—OH) present at the interface form hydrogen bonds with water (Scheme 3 in Musso et al., 2015). Many experimental and molecular-simulation studies on mesoporous silica and related materials (Vycor, MCM-41, and others) (Smirnov et al., 2000; Bellissent-Funel, 2002; Gallo et al., 2002; Crupi et al., 2003; Takahara et al., 2005; Yumaguchi et al., 2007; Mancinelli et al., 2009; Jelassi et al., 2011; Yoshida et al., 2012) suggest a strong reduction of the tetrahedral order (water–silica H-bonds substitute the water–water H-bonds), leading to the distortion of the H-bond network and a slow dynamics of confined water, affected by both the nature of the geometrical confinement and the interaction forces at the pore walls (Bellissent-Funel, 2005, 2008; Jelassi et al., 2010). A decrease in pore size leads to increasing distortion of the tetrahedral water structure and/or breaking down of hydrogen bonds among water molecules in confined water (Smirnov et al., 2000).

The infrared (IR) spectrum of liquid water consists of four main bands: (a) stretching motion of the covalent intramolecular OH bands (~3400 $cm^{-1}$) sensitive to the H-bonding environment; (b) the intramolecular HOH bending band (~1650 $cm^{-1}$) not sensitive to H-bonds; (c) the intermolecular libration band (~675 $cm^{-1}$) or frustrated rotation, associated with the rupture and rearrangement of the H-bonds; and (d) the connectivity/hindered translation band (~200 $cm^{-1}$) that characterizes the level of H-bonding between neighboring water molecules (e.g., Bergonzi and Mercury, 2013). The vibrational mode associated with stretching motion of the intramolecular OH bond is sensitive to the strength of H-bonding between molecules and the wavenumber increases (blue-shifts) with increasing distance between O atoms of two molecules linked by an H-bond, when local coordination weakens (e.g., Bratos et al., 2009). This stretching OH band can be divided into three Gaussian components, ascribed to three different

types of water molecules. From lower to higher frequencies these are: (a) fully coordinated Network Water (NW); (b) Intermediate Water (IW) with a coordination number close to two; and (c) Multimer Water (MW) with a low coordination number (e.g., Le Caër et al., 2011; Bergonzi and Mercury, 2013).

Huang et al. (2009) studied Raman spectra of water within the mesoporous Vycor glass (average pore diameter: 6.9 nm) during both adsorption and desorption processes. Reversible red-shifts and blue-shifts in the OH stretching frequency (between $\sim$3400 $cm^{-1}$ and $\sim$3500 $cm^{-1}$) were observed with increasing hydration levels during adsorption and decreasing hydration during desorption, respectively. Upon dehydration, the relative proportion of the fully coordinated NW component decreases, reflecting weaker and less ordered H-bonds with surrounding water molecules. Similar red-shifts with increasing hydration levels were also observed on other materials (porous $SiO_2$, $\gamma$-$Al_2O_3$, GelSil, NaA zeolite, and sodium bis-(2-ethylhexyl) sulfosuccinate reverse micelles) (Onori and Santucci, 1993; Goodman et al., 2001; Al-Abadleh and Grassian, 2003; Crupi et al., 2005).

### 6.2. Isotope fractionation of interfacial/confined water

The evidence from experimental and simulation studies discussed above strongly suggests a distorted H-bond network of adsorbed/confined water in porous materials and a red-shift in the OH-stretching vibrational frequency upon the hydration of porous materials, such as the mesoporous silica used in this study. As discussed by Jancso and Van Hook (1973), the red-shift in the OH stretching frequencies does occur upon condensation, decreasing the reduced partition function ratios for isotopes due to a "compression" of the difference in the zero-point energy ($\Delta$ZPE), namely an inverse isotope effect ($\alpha < 1$). However, three rather large librational frequencies appear upon condensation in the rotational–vibrational spectrum of water due to stronger intermolecular H-bonding in the liquid (e.g., Gupta and Meuwly, 2013). Therefore, the net isotope effect upon condensation of water remains normal ($\alpha > 1$) (Jancso and Van Hook, 1973).

We observed that the values of both $\alpha(^2H)$ and $\alpha(^{18}O)$ in the fully hydrated mesoporous silica (15 nm) are smaller than those of bulk liquid water and that they decrease with decreasing $p/p_o$. These experimental observations are consistent with the red-shift of the OH frequency upon condensation (or blue-shift upon dehydration), indicating the growth of more coordinated NW components with stronger H-bond network upon condensation. The fully coordinated NW component with lower frequency has a Gaussian peak close to that of ice (3250 $cm^{-1}$), while the IW component with a coordination number of two has a peak close to that of liquid water (3400 $cm^{-1}$). The high-frequency MW component with low coordination number has a peak close to that of vapor (3500 $cm^{-1}$) (Bergonzi and Mercury, 2013).

Huang et al. (2009) observed that the fractions of the fully coordinated NW and low-coordinated MW decrease and increase rapidly, respectively, with decreasing fraction of filled pores. The fraction of IM remains nearly constant. The observed patterns of $\alpha(^2H)$ and $\alpha(^{18}O)$ varying with the proportions of filled pores ($f$) in this study (Fig. 7) are very similar to the change in the fractions of NW with water contents (Huang et al., 2009). Using data of the area fractions of NW, IW, and MW water on Vycor (pore diameter: 6.9 nm) at different filling fractions (Huang et al., 2009), we have estimated for our porous silica sample (15 nm diameter): NW = 0, IW = 0, and MW = 1 at the monolayer stage ($p/p_o$ near 0); NW = 0.605, IW = 0.375, and MW = 0.02 near saturation ($p/p_o \sim 1$); and NW = 0.405, IW = 0.375, and MW = 0.22 at the hysteresis ($p/p_o \sim 0.8$). Applying the area fractions and our experimental results of $\alpha(^2H)$ and $\alpha(^{18}O)$ between adsorbed water in the porous silica and water vapor at the corresponding $p/p_o$ values ($1.01 \pm 0.01$ and $1.003 \pm 0.002$ at $p/p_o \sim 0$, 1.063 and 1.0083 at $p/p_o = 1$, and 1.045 and 1.0065 at $p/p_o = 0.82$ for $\alpha(^2H)$ and $\alpha(^{18}O)$ values, respectively), we obtained the equilibrium fractionation factors between the three components of the pore water and vapor: $1.01 \pm 0.01$ (MW), $1.01 \pm 0.01$ (IW), and $1.10 \pm 0.01$ (NW) for $\alpha(^2H)$ and $1.003 \pm 0.002$ (MW), $1.003 \pm 0.003$ (IW), and $1.012 \pm 0.002$ (NW) for $\alpha(^{18}O)$. For comparison, $\alpha(^2H)$ and $\alpha(^{18}O)$ values for liquid–vapor equilibrium is 1.074 and 1.0088 (this study; Horita and Wesolowski, 1994) and values for ice-vapor equilibrium are 1.133 and 1.0145 at 0 °C (Ellehoj et al., 2013). Our estimated fractionation factors for "ice-like" NW are indeed close to ice-vapor fractionation factors. However, the estimated values for "liquid-like" IW and "vapor-like" MW, which are very close to each other, are much closer to those of vapor rather than to those of liquid water.

## 7. IMPLICATIONS

Processes of isotope fractionation in soils have important implications for our understanding of terrestrial hydrology in general. Firstly, the stable isotopic composition of soil water has been used to trace water movements within the thick vadose zone, estimate the evaporation rate, and trace groundwater recharge (Allison and Barnes, 1983; Barnes and Allison, 1988; Cane and Clark, 1999; Gat, 2010). Secondly, the isotopic composition of soil water is useful to identify plant water sources (e.g., Ehleringer et al., 1999; Huang and Zhang, 2015) since the isotopic composition of water in stems and roots usually reflect the isotopic composition of plant-available soil water (Flanagan and Ehleringer, 1991). At the regional and global scale, the isotope composition of soil water can be used to explore land–atmosphere interactions (e.g., Hoffmann et al., 2000), to constrain primary productivity and ecosystem exchange (e.g., Welp et al., 2011; Werner et al., 2012), and to reconstruct the past environmental and climate parameters (surface temperature and relative humidity) (e.g., Helliker and Richter, 2008; Oerter et al., 2014). The results from this study, revealing that equilibrium isotope fractionation factors between adsorbed water in the mesoporous silica and water vapor differ significantly from those of bulk water liquid–vapor, prompt us to re-examine several major issues of vadose-zone isotope hydrology.

### 7.1. Analytical methods for the isotopic composition of soil water

Conventional analytical methods for the isotopic composition of soil water include the extraction of soil water by techniques such as high-pressure squeezing, vacuum distillation, or high speed centrifugation from soil (Gilg et al., 2004). These processes are time-consuming and suffer from possible sampling-induced fractionation when water from the soil matrices is not recovered quantitatively (Wassenaar et al., 2008; Garvelmann et al., 2012). Hsieh et al. (1998) tested the direct $H_2O$–$CO_2$ equilibration method for the $\delta^{18}O$ analysis of soil water. McConville et al. (1999) and Koehler et al. (2000) measured $\delta^2H$ of pore waters from clay-rich soil samples by equilibration of the sample with $H_2$, using a Pt catalyst at 25 °C. Wassenaar et al. (2008) developed pore water $H_2O_{(liquid)}$–$H_2O_{(vapor)}$ equilibration technique followed by isotope analysis of vapor samples by laser spectroscopy. This $H_2O_{(liquid)}$–$H_2O_{(vapor)}$ pore water equilibration with laser spectroscopy has advantages, including field-based hydrogeologic profiling (Garvelmann et al., 2012).

The equilibration methods discussed above have potential problems. In Hsieh et al. (1998) and Wassenaar et al. (2008), the effect of water contents on the $\delta^2H$ and $\delta^{18}O$ values of soil water was investigated by adding different amounts of water with a known isotopic composition to the soil sample. The measured isotopic compositions of soil water systematically change with water contents. Hsieh et al. (1998) suggested that water in soils may be partitioned into different "compartments" or "pools" such as bulk liquid water, water adsorbed onto mineral surfaces and organic matter, and structural water bound in minerals, each with different isotopic compositions. The isotopic composition of soil water calculated using a fractionation factor between $CO_2$/$H_2$/water vapor and liquid water is an operationally defined value for a liquid water "compartment" (Hsieh et al., 1998). Our study shows that the equilibrium isotope fractionation factors between adsorbed/confined water in the mesoporous silica and water vapor are smaller than those of bulk liquid water–vapor.

### 7.2. Multiple subsurface water pools with different isotopic compositions

Recent stable isotope studies reveal that two separate water bodies with different isotopic characteristics exist in trees and streams (Brooks et al., 2010; Goldsmith et al., 2012). Plant xylem water has similar stable isotope values as soil water, while the stream and ground water has similar stable isotope values as precipitation. The two pools of subsurface water were distinguished: the former is a pool of tightly bound soil water from precipitation, which is then taken up by plants, and the latter is a highly mobile precipitation pool that quickly infiltrates through the highly porous soil and eventually contributes to the stream. They attributed the differences in $\delta^{18}O$ and $\delta^2H$ values between the two pools to evaporation. They also observed that the isotope compositions of soil waters varied parallel to the local meteoric water line, with soil water at depth having lower isotope ratios than those of the upper soil, stream water and annual average precipitation.

Due to the interactions between matric and gravitational potential, the smallest pores are the last to drain and contain water that is relatively immobile compared with water in larger pores (Selker et al., 1999). Brooks et al. (2010) measured mobile soil water and bulk soil water (containing both mobile and matrix-bound water) collected at the same depth and location. They found that bulk soil water was always more depleted in heavy isotopes than mobile water, indicating that matrix-bound water is more depleted in heavy isotopes than mobile water. Oerter et al. (2014) suggested that the cation isotope effect of clay minerals under dry conditions may be relevant to the isotopic composition of plant available water in soils. Our results suggest that adsorbed/confined water in pores of different sizes in soils may have different isotopic compositions due to the effect of hydrophilic interaction between the water molecules and the pore surfaces.

### 7.3. Evaporation models

Due to practical difficulties in sampling soil water vapor, the isotopic composition of soil vapor or evaporation flux has traditionally been modeled rather than measured. In situ, direct isotope analysis of soil vapor by laser spectroscopy (Soderberg et al., 2011) is likely to be affected by sampling-induced mixing/evaporation within soils. Measurements of the isotopic composition of water vapor flux above ground (Yakir and Sternberg, 2000; Yepez et al., 2003; Wang et al., 2010) suffer from the difficulty in differentiating the evaporation flux from bare ground and the transpiration flux from vegetation within the area (Rothfuss et al., 2010; Wang et al., 2010; Good et al., 2012).

The Craig-Gordon evaporation model (Craig and Gordon, 1965), which was originally developed to calculate the isotopic composition of the evaporation flux from an open water body, has been extensively applied without modification to evapotranspi $\alpha_K$ ration from bare soils and vegetation:

$$\delta_E = \frac{\left(\frac{1}{\alpha_{L-V}}\right)\cdot\delta_L - \hbar\cdot\delta_A - (\varepsilon^* + \varepsilon_K)}{(1-\hbar) + 10^{-3}\varepsilon_K} \quad (4)$$

where $\delta_E$, $\delta_L$ and $\delta_A$ are the isotopic compositions of an evaporation flux, liquid water, and the "free atmospheric" water vapor, respectively. $\hbar = h/\alpha_{H_2O}$, where $h$ is the relative humidity of ambient air normalized to the saturation vapor pressure at the temperature of the water surface and $\alpha_{H_2O}$ is the activity of water. The $\varepsilon_K = 10^3(1-\alpha_K)$, where is the kinetic fractionation factor, representing a bundled, total kinetic isotope effect that arises from the transport of water vapor through the three layers (interface, laminar layer and turbulent section).

Natural and experimental studies for depth profiles of the isotopic composition of water in soils under evaporitic environments showed maximum enrichments of heavy isotopes ($^1H^2HO$ and $^2H^{18}O$) at the water–air interface of soil columns by evaporation and an exponential decrease with

depth by diffusional transport. Much smaller slopes (2.6–3.4) were observed for soil water in the $\delta^2$H-$\delta^{18}$O diagram, compared to the slopes (4–6) of evaporitic open water bodies (Zimmermann et al., 1967; Gat, 1971; Allison et al., 1983). The isotopic composition of leaf water is also characterized by high and variable degrees of the enrichments of $^1H^2HO$ and $^2H^{18}O$ with smaller slopes (1.5–2.5) in the $\delta^2$H-$\delta^{18}$O diagram (Allison et al., 1985). These isotopic profiles within soils and leaves have been interpreted within the framework of the Craig-Gordon model. The Craig-Gordon evaporation model has been further incorporated into numerical land-surface isotope models such as SiSPAT-Isotope and Soil-Litter-Iso to model the isotopic composition of regional to global soil moisture (Shurbaji and Phillips, 1995; Mathieu and Bariac, 1996; Melayah et al., 1996; Braud et al., 2005, 2009; Haverd and Cuntz, 2010).

In applications of the Craig-Gordon model to soil water, the fundamental assumption that the liquid–vapor phase transition of soil water in the vadose zone has the same isotope fractionation as for bulk water ($\alpha_{L-V}$ in Eq. (4)). Our experimental results in this study demonstrated that the equilibrium isotope fractionation factors between adsorbed water in the mesoporous (15 nm diameter) silica and water vapor are significantly smaller than those of bulk liquid water, affected by the interaction between the water molecules and the hydrophilic pore surface. Thus, in the application of Craig-Gordon evaporation model (Eq. (4)) to soil (and plant) water, the equilibrium isotope fractionation between water vapor and adsorbed/pore-condensed water within porous materials (soils and plant tissue), varying with pore sizes and saturation levels, cannot be assumed the same as that between bulk liquid water and vapor. The equations developed for the mesoporous silica (15 nm) (Eqs. (2) and (3)) may be used as guidance for silica-rich soils.

## 8. CONCLUSIONS

Our experiments on equilibrium isotope fractionation between adsorbed water in the mesoporous silica (pore diameter: 15 nm) and water vapor at 30 °C demonstrated that equilibrium isotope fractionation factors $\alpha(^2H)$ and $\alpha(^{18}O)$ at $p/p_o = 1$ are lower than those of bulk water and decrease rapidly with decreasing $p/p_o$. These isotope effects of interfacial/confined water are caused by the weakened hydrogen-bond network due to hydrophilic interactions with the silica surface relative to bulk liquid water. Of the three components of pore waters (MW, IM, and NW), low-coordinated MW and fully-coordinated NW are indeed "vapor-like" and "ice-like," respectively, in terms of their reduced partition function ratios. However, IM behaves more "vapor-like" rather than "liquid-like."

Our results suggest that the long-held assumption in modeling the isotopic composition of soil water in vadose zones may not be valid. The equilibrium isotope fractionation between adsorbed/pore condensed water within soils and water vapor is not the same as that for bulk liquid water–water vapor system. Our results also have implications for improving the equilibration methods to obtain the isotopic compositions of soil water and for understanding different pools of subsurface water that contribute to plants and streams. Further experiments are needed on different materials (silica, alumina, clay) with different pore sizes to fully understand the cause of the observed isotope effects of water at interface and in confinement and to generate model equations that can be readily applied to soil water in arid and semi-arid zones.

## ACKNOWLEDGEMENTS

The authors thank C. Liu for his help in the TC/EA setup for isotope analysis of water, B. Zhao for the SEM image, and M. Ridley for the $N_2$ isotherm. The authors thank AE E. Schauble for handling the manuscript and making corrections. We appreciate constructive comments from three anonymous reviewers, which improved the manuscript greatly. This project is fully funded by NSF/EAR 1316228. Y.L. acknowledges the Institute of Deep-sea Science and Engineering, Chinese Academy of Sciences for supplemental financial support. We are grateful to the Texas Tech University Graduate Student Writing Center for assistance in editing.

## REFERENCES

Al-Abadleh H. A. and Grassian V. H. (2003) FT-IR study of water adsorption on aluminum oxide surfaces. *Langmuir* **19**, 341–347.

Allison G. B. and Barnes C. J. (1983) Estimation of evaporation from non-vegetated surfaces using natural deuterium. *Nature* **301**, 143–145.

Allison G. B., Barnes C. J. and Hughes M. W. (1983) The distribution of deuterium and $^{18}O$ in dry soils. 2. Experimental. *J. Hydrol.* **64**, 377–397.

Allison G. B., Gat J. R. and Leaney F. W. J. (1985) The relationship between deuterium and O-18 delta values in leaf water. *Chem. Geol.* **58**, 145–156.

Barnes C. J. and Allison G. B. (1988) Tracing of water-movement in the unsaturated zone using stable isotopes of hydrogen and oxygen. *J. Hydrol.* **100**, 143–176.

Bellissent-Funel M. C. (2002) Water near hydrophilic surfaces. *J. Mol. Liq.* **96–97**, 287–304.

Bellissent-Funel M. C. (2005) Hydrophilic-hydrophobic interplay: from model systems to living systems. *C.R. Geosci.* **337**, 173–179.

Bellissent-Funel M. C. (2008) Effects of pressure and confinement on liquid water. *J. Phys.-Condens. Mat.* **20**, 244120.

Bergonzi I. and Mercury L. (2013) Infrared-thermodynamics conversion as a function of temperature: towards confined water. In *Transport and Reactivity of Solutions in Confined Hydrosystems* (eds. L. Mercury, N. Tas and M. Zilberbrand). Springer, pp. 43–53.

Bratos S., Leicknam J. C. and Pommeret S. (2009) Relation between the OH stretching frequency and the OO distance in time-resolved infrared spectroscopy of hydrogen bonding. *Chem. Phys.* **359**, 53–57.

Braud I., Bariac T., Gaudet J. P. and Vauclin M. (2005) SiSPAT-Isotope, a coupled heat, water and stable isotope (HDO and $H_2{}^{18}O$) transport model for bare soil. Part I. Model description and first verifications. *J. Hydrol.* **309**, 277–300.

Braud I., Biron P., Bariac T., Richard P., Canale L., Gaudet J. P. and Vauclin M. (2009) Isotopic composition of bare soil evaporated water vapor. Part I: RUBIC IV experimental setup and results. *J. Hydrol.* **369**, 1–16.

Brooks J. R., Barnard H. R., Coulombe R. and McDonnell J. J. (2010) Ecohydrologic separation of water between trees and streams in a Mediterranean climate. *Nat. Geosci.* **3**, 100–104.

Burnett M. G., Galwey A. K. and Lawther C. (1996) Ideality of water vapour and its adsorption on the glass surfaces of a conventional glass vacuum apparatus at 295 K between 0 and 10 Torr. *J. Chem. Soc. Faraday Trans.* **92**, 4301–4304.

Cane G. and Clark I. D. (1999) Tracing ground water recharge in an agricultural watershed with isotopes. *Ground Water* **37**, 133–139.

Chen H., Wang J. H., Rahman Z. U., Worden J. G., Liu X., Dai Q. and Huo Q. (2007) Beach sand from Cancun Mexico: a natural macro- and mesoporous material. *J. Mater. Sci.* **42**, 6018–6026.

Coplen T. B. and Hanshaw B. B. (1973) Ultrafiltration by a compacted clay membrane. 1. Oxygen and hydrogen isotopic fractionation. *Geochim. Cosmochim. Acta* **37**, 2295–2310.

Craig H. and Gordon L. I. (1965) Deuterium and oxygen 18 variations in the ocean and the marine atmosphere. In *Stable Isotopes in Oceanographic Studies and Paleotemperatures* (ed. E. Tongiorgi). Laboratorio di Geologia Nucleare, Pisa, pp. 9–130.

Crupi V., Majolino D., Migliardo P., Venuti V. and Bellissent-Funel M. C. (2003) Structure and dynamics of water confined in a nanoporous sol-gel silica glass: a neutron scattering study. *Mol. Phys.* **101**, 3323–3333.

Crupi V., Majolino D., Migliardo P. and Venuti V. (2005) Dynamical properties of liquids in restricted geometries. *J. Mol. Liq.* **117**, 165–171.

Duniway M. C., Herrick J. E. and Monger H. C. (2007) The high water-holding capacity of petrocalcic horizons. *Soil Sci. Soc. Am. J.* **71**, 812–819.

Ehleringer J. R., Schwinning S. and Gebauer R. (1999) Water use in arid land ecosystems. In *Physiological Plant Ecology* (eds. M. C. Press, J. D. Scholes and M. G. Barker). Blackwell Science, Oxford, UK, pp. 347–365.

Ellehoj M. D., Steen-Larsen H. C., Johnsen S. J. and Madsen M. B. (2013) Ice-vapor equilibrium fractionation factor of hydrogen and oxygen isotopes: experimental investigations and implications for stable water isotope studies. *Rapid Commun. Mass Spectrometry* **27**, 2149–2158.

Feng S. and Fu Q. (2013) Expansion of global drylands under a warming climate. *Atmos. Chem. Phys.* **13**, 10081–10094.

Feng X. H. and Savin S. M. (1993) Oxygen-isotope studies of zeolites stilbite, analcime, heulandite, and clinoptilolite. 3. Oxygen-isotope fractionation between stilbite and water or water-vapor. *Geochim. Cosmochim. Acta* **57**, 4239–4247.

Ferreiro J. P., Miranda J. G. V. and Vazquez E. V. (2010) Multifractal analysis of soil porosity based on mercury injection and nitrogen adsorption. *Vadose Zone J.* **9**, 325–335.

Flanagan L. B. and Ehleringer J. R. (1991) Stable isotope composition of stem and leaf water: applications to the study of plant water-use. *Funct. Ecol.* **5**, 270–277.

Flint A. L., Campbell G. S., Ellett K. M. and Calissendorff C. (2002) Calibration and temperature correction of heat dissipation matric potential sensors. *Soil Sci. Soc. Am. J.* **66**, 1439–1445.

Gallo P., Rapinesi M. and Rovere M. (2002) Confined water in the low hydration regime. *J. Chem. Phys.* **117**, 369–375.

Garvelmann J., Kulls C. and Weiler M. (2012) A porewater-based stable isotope approach for the investigation of subsurface hydrological processes. *Hydrol. Earth Syst. Sci.* **16**, 631–640.

Gat J. R. (1971) Comments on stable isotope method in regional groundwater investigations. *Water Resour. Res.* **7**, 980–993.

Gat J. R. (2010) *Isotope Hydrology: A Study of the Water Cycle*. Imperical College Press.

Gilg H. A., Girard J.-P. and Sheppard S. M. F. (2004) Conventional and less conventional techniques for hydrogen and oxygen isotope analysis of clays, associated minerals and pore waters in sediments and soils. In *Handbooks of Stable Isotope Analytical Techniques*, vol. 1 (ed. P. A. de Groot), pp. 38–61. Handbooks of Stable Isotope Analytical Techniques. Elsevier Science B.V., Amsterdam.

Goldsmith G. R., Muñoz-Villers L. E., Holwerda F., McDonnell J. J., Asbjornsen H. and Dawson T. E. (2012) Stable isotopes reveal linkages among ecohydrological processes in a seasonally dry tropical montane cloud forest. *Ecohydrology* **5**, 779–790.

Good S. P., Soderberg K., Wang L. X. and Caylor K. K. (2012) Uncertainties in the assessment of the isotopic composition of surface fluxes: a direct comparison of techniques using laser-based water vapor isotope analyzers. *J. Geophys. Res.-Atmos.* **117**, D15301.

Good S. P., Noone D. and Bowen G. (2015) Hydrologic connectivity constrains partitioning of global terrestrial water fluxes. *Science* **349**, 175–177.

Goodman A. L., Bernard E. T. and Grassian V. H. (2001) Spectroscopic study of nitric acid and water adsorption on oxide particles: enhanced nitric acid uptake kinetics in the presence of adsorbed water. *J. Phys. Chem. A* **105**, 6443–6457.

Grace J., San Jose J., Meir P., Miranda H. S. and Montes R. A. (2006) Productivity and carbon fluxes of tropical savannas. *J. Biogeogr.* **33**, 387–400.

Gregg S. G. and Sing K. S. W. (1982) *Adsorption, Surface Area and Porosity*. Academic Press.

Gruszkiewicz M. S., Horita J., Simonson J. M., Mesmer R. E. and Hulen J. B. (2001) Water adsorption at high temperature on core samples from The Geysers geothermal field, California, USA. *Geothermics* **30**, 269–302.

Gupta P. K. and Meuwly M. (2013) Dynamics and vibrational spectroscopy of water at hydroxylated silica surfaces. *Faraday Discuss.* **167**, 329–346.

Hajnos M., Lipiec J., Swieboda R., Sokolowska Z. and Witkowska-Walczak B. (2006) Complete characterization of pore size distribution of tilled and orchard soil using water retention curve, mercury porosimetry, nitrogen adsorption, and water desorption methods. *Geoderma* **135**, 307–314.

Harvey A. H. (1998) *Thermodynamic Properties of Water: Tabulation from the IAPWS Formulation 1995 for the Thermodynamic Properties of Ordinary Water Substance for General and Scientific Use*. National Institute of Standards and Technology Report NISTIR 5078.

Haverd V. and Cuntz M. (2010) Soil-Litter-Iso: a one-dimensional model for coupled transport of heat, water and stable isotopes in soil with a litter layer and root extraction. *J. Hydrol.* **388**, 438–455.

Helliker B. R. and Richter S. L. (2008) Subtropical to boreal convergence of tree-leaf temperatures. *Nature* **454**, 511–514.

Hoffmann G., Jouzel J. and Masson V. (2000) Stable water isotopes in atmospheric general circulation models. *Hydrol. Process.* **14**, 1385–1406.

Horita J. and Wesolowski D. J. (1994) Liquid–vapor fractionation of oxygen and hydrogen isotopes of water from the freezing to the critical-temperature. *Geochim. Cosmochim. Acta* **58**, 3425–3437.

Hsieh J. C. C., Savin S. M., Kelly E. F. and Chadwick O. A. (1998) Measurement of soil-water $\delta^{18}O$ values by direct equilibration with $CO_2$. *Geoderma* **82**, 255–268.

Huang L. and Zhang Z. S. (2015) Stable isotopic analysis on water utilization of two xerophytic shrubs in a revegetated desert area: Tengger Desert, China. *Water* **7**, 1030–1045.

Huang X. F., Wang Q., Liu X. X., Yang S. H., Li C. X., Sun G., Pan L. Q. and Lu K. Q. (2009) Vibrational dynamics of water within mesoporous materials at different hydration levels during adsorption and desorption processes. *J. Phys. Chem. C* **113**, 18768–18771.

Jancso G. and Van Hook W. A. (1973) Condensed phase isotope effects (especially vapor pressure isotope effects). *Chem. Rev.* **74**, 689–750.

Jelassi J., Castricum H. L., Bellissent-Funel M. C., Dore J., Webber J. B. W. and Sridi-Dorbez R. (2010) Studies of water and ice in hydrophilic and hydrophobic mesoporous silicas: pore characterisation and phase transformations. *Phys. Chem. Chem. Phys.* **12**, 2838–2849.

Jelassi J., Grosz T., Bako I., Bellissent-Funel M. C., Dore J. C., Castricum H. L. and Sridi-Dorbez R. (2011) Structural studies of water in hydrophilic and hydrophobic mesoporous silicas: an X-ray and neutron diffraction study at 297 K. *J. Chem. Phys.* **134**, 064509.

Karlsson H. R. (2001) Isotope geochemistry of zeolites. *Rev. Mineral. Geochem.* **45**, 163–205.

Karlsson H. R. and Clayton R. N. (1990) Oxygen isotope fractionation between analcime and water – an experimental-study. *Geochim. Cosmochim. Acta* **54**, 1359–1368.

Koehler G., Wassenaar L. I. and Hendry M. J. (2000) An automated technique for measuring δD and $\delta^{18}O$ values of porewater by direct $CO_2$ and $H_2$ equilibration. *Anal. Chem.* **72**, 5659–5664.

Le Caër S., Pin S., Esnouf S., Raffy Q., Renault J. P., Brubach J. B., Creff G. and Roy P. (2011) A trapped water network in nanoporous material: the role of interfaces. *Phys. Chem. Chem. Phys.* **13**, 17658–17666.

Likos W. J. and Lu N. (2006) Pore-scale analysis of bulk volume change from crystalline interlayer swelling in $Na^+$- and $Ca^{2+}$-smectite. *Clays Clay Miner.* **54**, 515–528.

Likos W. J., Lu N. and Wenszel W. (2011) Performance of a dynamic dew point method for moisture isotherms of clays. *Geotech. Test J.* **34**, 373–382.

Lowell S., Shields J. E., Thomas M. A. and Thommes M. (2010) *Characterization of Porous Solids and Powders: Surface Area, Pore Size, and Density*. Kluwer Academic Publishers, Dordrecht, The Netherlands.

Lu S.-G., Malik Z., Chen D.-P. and Wu C.-F. (2014) Porosity and pore size distribution of Ultisols and correlations to soil iron oxides. *Catena* **123**, 79–87.

Mancinelli R., Imberti S., Soper A. K., Liu K. H., Mou C. Y., Bruni F. and Ricci M. A. (2009) Multiscale approach to the structural study of water confined in MCM41. *J. Phys. Chem. B* **113**, 16169–16177.

Mathieu R. and Bariac T. (1996) A numerical model for the simulation of stable isotope profiles in drying soils. *J. Geophys. Res.-Atmos.* **101**, 12685–12696.

McConville C., Kalin R. M. and Flood D. (1999) Direct equilibration of soil water for delta O-18 analysis and its application to tracer studies. *Rapid Commun. Mass Spectrometry* **13**, 1339–1345.

Melayah A., Bruckler L. and Bariac T. (1996) Modeling the transport of water stable isotopes in unsaturated sails under natural conditions. 1. Theory. *Water Resour. Res.* **32**, 2047–2054.

Musso G. E., Bottinelli E., Celi L., Magnacca G. and Berlier G. (2015) Influence of surface functionalization on the hydrophilic character of mesoporous silica nanoparticles. *Phys. Chem. Chem. Phys.* **17**, 13882–13894.

Naono H. and Hakuman M. (1991) Analysis of adsorption-isotherms of water-vapor for nonporous and porous adsorbents. *J. Colloid Interf. Sci.* **145**, 405–412.

Naono H. and Hakuman M. (1993) Analysis of porous texture by means of water-vapor adsorption-isotherm with particular attention to lower limit of hysteresis loop. *J. Colloid Interf. Sci.* **158**, 19–26.

Naono H., Hakuman M., Tanaka T., Tamura N. and Nakai K. (2000) Porous texture and surface character of dehydroxylated and rehydroxylated MCM-41 mesoporous silicas – analysis of adsorption isotherms of nitrogen gas and water vapor. *J. Colloid Interf. Sci.* **225**, 411–420.

Naumov S. (2009) *Hysteresis phenomena in mesoporous materials* (Ph.D. thesis). University of Leipzig, Leipzig, Germany.

Nielsen M. E. and Fisk M. R. (2010) Surface area measurements of marine basalts: implications for the subseafloor microbial biomass. *Geophys. Res. Lett.* **37**, L15604.

Noto M. and Kusakabe M. (1997) An experimental study of oxygen isotope fractionation between wairakite and water. *Geochim. Cosmochim. Acta* **61**, 2083–2093.

Oerter E., Finstad K., Schaefer J., Goldsmith G. R., Dawson T. and Amundson R. (2014) Oxygen isotope fractionation effects in soil water via interaction with cations (Mg, Ca, K, Na) adsorbed to phyllosilicate clay minerals. *J. Hydrol.* **515**, 1–9.

O'Neil J. R. (1986) Theoretical and experimental aspects of isotopic fractionation. In *Stable Isotopes in High Temperature Geological Processes* (eds. J. W. Valley, H. P. Taylor and J. R. O'Neil). Rev. Mineral. pp. 11–40.

Onori G. and Santucci A. (1993) Ir investigations of water-structure in Aerosol OT reverse micellar aggregates. *J. Phys. Chem.* **97**, 5430–5434.

Richard T., Mercury L., Massault M. and Michelot J. L. (2007) Experimental study of D/H isotopic fractionation factor of water adsorbed on porous silica tubes. *Geochim. Cosmochim. Acta* **71**, 1159–1169.

Rothfuss Y., Biron P., Braud I., Canale L., Durand J. L., Gaudet J. P., Richard P., Vauclin M. and Bariac T. (2010) Partitioning evapotranspiration fluxes into soil evaporation and plant transpiration using water stable isotopes under controlled conditions. *Hydrol. Process.* **24**, 3177–3194.

Scanlon B. R. (2000) Uncertainties in estimating water fluxes and residence times using environmental tracers in an arid unsaturated zone. *Water Resour. Res.* **36**, 395–409.

Scanlon B. R., Tyler S. W. and Wierenga P. J. (1997) Hydrologic issues in arid, unsaturated systems and implications for contaminant transport. *Rev. Geophys.* **35**, 461–490.

Selker J. S., Keller C. K. and McCord J. T. (1999) *Vadose Zone Processes*. Lewis Publishers, Boca Raton, Fla.

Shurbaji A. R. M. and Phillips F. M. (1995) A numerical-model for the movement of $H_2O$, $H_2{}^{18}O$, and $^2HHO$ in the unsaturated zone. *J. Hydrol.* **171**, 125–142.

Sing K. S. W., Everett D. H., Haul R. A. W., Moscou L., Pierotti R. A., Rouquerol J. and Siemieniewska T. (1985) Reporting physisorption data for gas solid systems with special reference to the determination of surface-area and porosity (Recommendations 1984). *Pure Appl. Chem.* **57**, 603–619.

Smirnov P., Yamaguchi T., Kittaka S., Takahara S. and Kuroda Y. (2000) X-ray diffraction study of water confined in mesoporous MCM-41 materials over a temperature range of 223–298 K. *J. Phys. Chem. B* **104**, 5498–5504.

Soderberg K., Good S. P., Wang L. and Caylor K. (2011) Stable isotopes of water vapor in the vadose zone: a review of measurement and modeling techniques. *Vadose Zone J.* **11**(3).

Stewart G. L. (1972) Clay-water interaction, behavior of $^3H$ and $^2H$ in adsorbed water, and isotope-effect. *Soil Sci. Soc. Am. Proc.* **36**, 421–426.

Takahara S., Sumiyama N., Kittaka S., Yamaguchi T. and Bellissent-Funel M. C. (2005) Neutron scattering study on dynamics of water molecules in MCM-41. 2. Determination of translational diffusion coefficient. *J. Phys. Chem. B* **109**, 11231–11239.

Walrafen G. (1981) Water: A Comprehensive Treatise, vol. 1. (ed. F. Franks). Plenum, New York, Chapter 5.

Wang L. X., Caylor K. K., Villegas J. C., Barron-Gafford G. A., Breshears D. D. and Huxman T. E. (2010) Partitioning evapotranspiration across gradients of woody plant cover: assessment of a stable isotope technique. *Geophys. Res. Lett.* **37**, L09401.

Wassenaar L. I., Hendry M. J., Chostner V. L. and Lis G. P. (2008) High resolution pore water δD and $\delta^{18}O$ measurements by $H_2O$ (liquid)–$H_2O$(vapor) equilibration laser spectroscopy. *Environ. Sci. Technol.* **42**, 9262–9267.

Welp L. R., Keeling R. F., Meijer H. A. J., Bollenbacher A. F., Piper S. C., Yoshimura K., Francey R. J., Allison C. E. and Wahlen M. (2011) Interannual variability in the oxygen isotopes of atmospheric $CO_2$ driven by El Nino. *Nature* **477**, 579–582.

Werner C., Schnyder H., Cuntz M., Keitel C. and Zeeman M. J., et al. (2012) Progress and challenges in using stable isotopes to trace carbon and water relations across scales. *Biogeosciences* **9**, 3083–3111.

Yakir D. and Sternberg L. D. L. (2000) The use of stable isotopes to study ecosystem gas exchange. *Oecologia* **123**(3), 297–311.

Yepez E. A., Williams D. G., Scott R. L. and Lin G. H. (2003) Partitioning overstory and understory evapotranspiration in a semiarid savanna woodland from the isotopic composition of water vapor. *Agric. Forest Meteorol.* **119**, 53–68.

Yoshida K., Yamaguchi T., Kittaka S., Bellissent-Funel M. C. and Fouquet P. (2012) Neutron spin echo measurements of monolayer and capillary condensed water in MCM-41 at low temperatures. *J. Phys.-Condens. Mat.* **24**, 064101.

Yumaguchi T., Yoshida K., Smirnov P., Takamuku T., Kittaka S., Takahara S., Kuroda Y. and Bellissent-Funel M.-C. (2007) Structure and dynamic properties of liquid confined in MCM-41 mesopores. *Eur. Phys. J. Special Topics* **141**, 19–27.

Zimmermann U., Ehhalt D. H. and Munnich K. O. (1967) Soil-water movement and evapotranspiration: changes in the isotopic composition of the water. In *Proceeding of the Symposium on Isotopes in Hydrology*. IAEA, pp. 567–585.

*Associate editor:* Edwin Schauble